Global view on a nonlinear oscillator subject to time-delayed feedback control

Hartmut Erzgräber [1] and Wolfram Just

School of Mathematical Sciences, Queen Mary / University of London, Mile End Road, London E1 4NS, UK

Abstract

We apply time-delayed feedback control to stabilise unstable periodic orbits of an amplitude-phase oscillator. The control acts on both, the amplitude and the frequency of the oscillator, and we show how the phase of the control signal influences the dynamics of the oscillator. A comprehensive bifurcation analysis in terms of the control phase and the control strength reveals large stability regions of the target periodic orbit, as well as an increasing number of unstable periodic orbits caused by the time delay of the feedback loop. Our results provide insight into the global features of time-delayed control schemes.

Key words: Time delay dynamics, Bifurcation analysis, Control of chaos
PACS: 02.30.Ks, 05.45.Gg, 02.30.Oz

1 Introduction

Control of chaos, that means the stabilisation of unstable orbits in complex dynamical systems using small control forces, has attracted considerable interest for the last 15 years. The field is still one of the most vibrant research areas in applied sciences. Applications cover such diverse fields like laser systems, biological networks, or chemical engineering (see for example Ref. [1] and references therein). A very powerful method introduced by Pyragas in Ref. [2] uses time-delayed feedback for the non-invasive control of periodic target states. This approach is of particular interest from the plain theoretical point of view as well, since dynamics with time delay plays an important role in various fields of science, see Refs. [3–7].

[1] permanent address: School of Engineering Computing and Mathematics, University of Exeter, North Park Road, Exeter EX4 4QF UK

Recent interest in the theory of time-delayed feedback control was mainly stimulated by analytic linear stability analysis of such systems [8,9]. In particular, it has been pointed out that certain types of periodic orbits are not accessible for time-delayed feedback methods [9,10], a claim which has been shown recently to be incorrect for autonomous systems [11]. In that context a generic nonlinear oscillator subjected to time-delayed feedback control has been introduced and the linear stability properties have been investigated in some detail [12].

There exists virtually no systematic investigation of time-delayed feedback control beyond the linear regime. To our best knowledge the sole result of general applicability proposes the transition form sub- to supercritical bifurcations for the estimation of basins of attraction [13]. Here, we are concerned with global features of time delay dynamics in general, and time-delayed feedback control in particular. To this end we present a systematic study of a generic model for time-delayed feedback control including stability properties of delay-induced states and of the bifurcating torus solutions, as well as global bifurcations.

The idea of time-delayed feedback control, as considered here, is to stabilize a certain target state (in our case a periodic orbit with a certain period), which otherwise would be unstable. In the simplest case, which is considered here, this unstable periodic arises from a subcritical Hopf normal from. In applications with more complex models more complicated and even chaotic dynamics can be expected in addition to the unstable periodic target orbit. However our simple model contains all the necessary structure to analyse the effects of time-delayed feedback for stabilization unstable periodic orbits.

Sec. 2 introduces the model equations and contains a discussion of basic properties. In Sec. 3 we present one-parameter bifurcation diagrams of the Pyragas mode and the control modes including a linear stability analysis. The stability domains in the parameter plane of control phase versus control strength are computed in Sec. 4. Here, we identify several codimension-two points, specifically Bogdanov-Takens points, as organising centres of the dynamics. We devote Sec. 5 to a more detailed discussion of the dynamics in a neighbourhood of these higher codimension bifurcation points. Conclusions and outlook are given in Sec 6.

2 The Model

We consider the control of an unstable Stuart-Landau oscillator by time-delayed feedback,

$$\dot{z}(t) = (\lambda + i)z(t) + (1 + i\gamma)|z(t)|^2 z(t) - K\exp(i\beta)[z(t) - z(t-\tau)]\,, \quad (1)$$

where z is a complex valued variable. This model, which has been introduced recently [11], describes the amplitude and phase dynamics of a nonlinear oscillator. It can be expected that Eq. (1) shows generic features since any dynamical system at the onset of an oscillation can be reduced to the normal form of a Hopf bifurcation with suitable normal form coefficients [14]. Time-delayed feedback control is implemented by a control signal proportional to the difference between the state at time t and time $t-\tau$ in the past, $z(t) - z(t-\tau)$. This difference becomes zero if and only if the system oscillates with period τ. The parameter K determines the control strength while the second control parameter β allows to change the phase relation between the oscillator and the feedback signal. In fact, the importance of the control parameter β for time-delayed feedback control has been pointed out recently in Ref. [11,15]. The extension from a one-parameter to a two-parameter control scheme enables the stabilisation of a larger class of periodic target states. Furthermore, the parameter β couples to the phase of the oscillator. While being of importance from the plain mathematical perspective, for many physical systems involving phase-amplitude dynamics such a phase parameter turns out to be essential for organising the dynamics, see for example Refs. [15,16,7,17]. Finally, even an experimental realisation of such coupling schemes seem to be feasible, either by taking a bivariate measured time series or by manipulating directly the phase in optical experiments. Even though the model (1) looks quite simple, analytical treatment is substantially hampered due to the time delay, in particular with regards to global bifurcations and bifurcations of nontrivial states. Here we use for such purposes the numerical continuation package DDE-BIFTOOL for delay differential equations, see Ref [18] and Refs. [16,19,20] for applications of numerical continuation.

Without control, i.e., $K = 0$ the model (1) reduces to the normal form of the subcritical Hopf bifurcation. Thus, an unstable limit cycle

$$z_P(t) = R_P \exp(i\Omega_P t) \quad (2)$$

occurs for $\lambda < 0$ where amplitude R_P and frequency Ω_P are given by

$$R_P = \sqrt{-\lambda}, \quad \Omega_P = 1 - \lambda\gamma \quad . \quad (3)$$

In order to stabilise this unstable harmonic oscillation delayed feedback control with a suitable choice of the control parameters K and β and the delay time τ must be applied. In particular, we choose the delay time τ such that it satisfies the Pyragas condition

$$\tau = \frac{2\pi}{\mid \Omega_P \mid} = \frac{2\pi}{\mid 1 - \gamma\lambda \mid} \quad . \quad (4)$$

This condition ensures that the limit cycle (2) still solves Eq. (1) and the control scheme is potentially non-invasive. Of course, depending on the value of the control amplitude K and the control phase β Eq. (1) may have additional periodic or aperiodic stationary states. Due to the rotational S^1-symmetry of the equation of motion, $z(t) \mapsto \exp(i\phi)z(t)$, there may occur other harmonic solutions $z(t) = R\exp(i\Omega t)$ where $R \neq R_P$ or $\Omega \neq \Omega_P$. We will call such solutions control modes because they represent harmonic oscillations induced by the control loop. Such control modes will be one of the key ingredient to understand the bifurcation scenario of Eq. (1).

We present a systematic bifurcation analysis of the structure and the stability of the Pyragas mode (2) and of the control modes of Eq. (1). For the parameters of the oscillator we adopt the values $\gamma = -10$ and $\lambda = (\pi - 4)/40 \approx -0.02$ which correspond to the period $\tau = 8$ according to the Pyragas condition (4). The control parameters K and β act as bifurcation parameters. The symmetry of these variables

$$(K, \beta) \mapsto (-K, \beta + \pi) \tag{5}$$

allows to restrict the control amplitude to positive values, $K \geq 0$. However, we do not exploit such a symmetry and consider for convenience both, positive and negative values of K.

3 Stability of the control modes

First we consider one-parameter bifurcation diagrams, keeping one of the parameters K or β fixed, and monitor the harmonic solutions of Eq. (1) in terms of their frequency Ω and amplitude R.

Figure 1 shows one-parameter bifurcation diagrams for fixed control strength $K = 0.15$ with the control phase β as free parameter. Panel (a) shows the frequency Ω of the periodic orbit as a function of β and panel (b) the amplitude R. Due to the symmetry (5) the diagram is 2π-periodic in the control phase β. Stable solutions are shown in thick (green) and unstable ones as thin (magenta) curves. Additionally, higher control modes are shown as thin black curves. Saddle-node bifurcations are marked by crosses (+), transcritical bifurcations by circles ($\circ$), Hopf bifurcations by stars ($*$), and Hopf bifurcations of the trivial solution $z_0 = 0$ by dots ($\bullet$). Moreover, in brackets are the numbers of positive eigenvalues, which indicates the dimension of the unstable manifold along the respective branches, where we restrict the labelling to one fundamental 2π-interval of the phase parameter β.

One can easily identify the Pyragas mode as a horizontal line with a constant

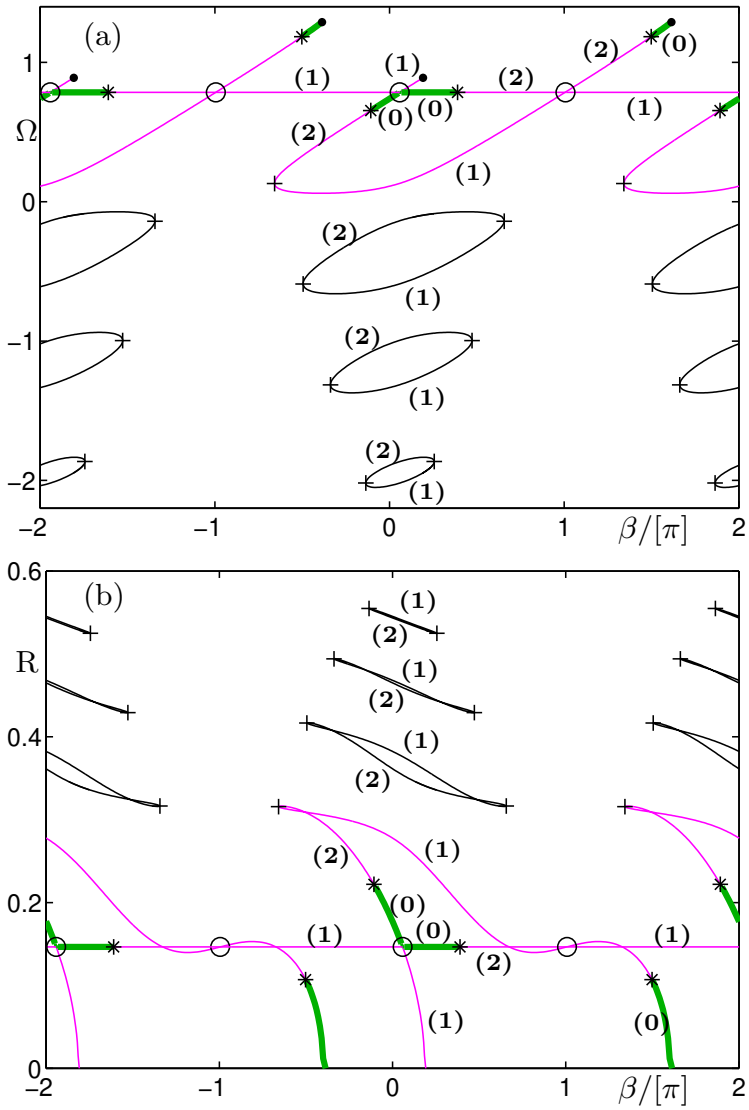

Fig. 1. One-parameter bifurcation diagram for $K = 0.15$ in the (β, Ω)-projection (a) and (β, R)-projection (b) . Stable solutions (green/thick), unstable solutions (magenta/thin), saddle-node bifurcations (crosses +), transcritical bifurcations (circles ∘), Hopf bifurcations (stars ∗), and Hopf bifurcations of the trivial solution (dots •). Higher control modes, which are all unstable, are indicated as thin black curves. In brackets are the numbers of positive eigenvalues indicating the dimension on the unstable manifold.

frequency of $\Omega_P = \pi/4 \approx 0.79$ in panel (a), and as a horizontal line with constant amplitude of $R_P = \sqrt{-\lambda} \approx 0.15$ in panel (b). Additional periodic orbits are born in pairs in saddle-node bifurcations. In our case all such saddle-node bifurcations are accompanied by a finite-dimensional transversal unstable manifold, i.e., the two solutions born in the saddle-node bifurcation are both of saddle type and their unstable dimension differs by one. According to their properties within the centre manifold we label the solution with lower number of positive eigenvalues as node-type and the other one as saddle-type. These

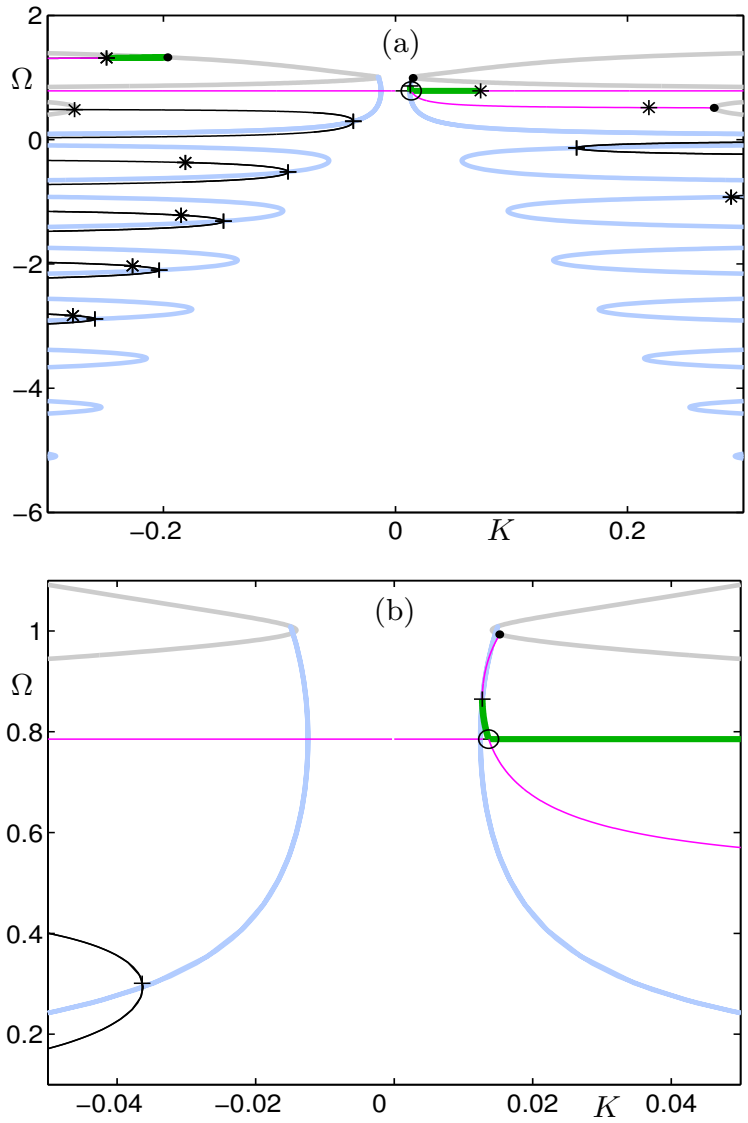

Fig. 2. One-parameter bifurcation diagram in the (K, Ω)-projection for $\beta = 2\pi/3$ (a) and enlarged view in a neighbourhood of the transcritical bifurcation (b). Light blue curves: the position of the saddle-node bifurcation in the (K, Ω)-projection parameterised by the control phase β, gray curve: the projection of the Hopf bifurcation curve of the trivial solution, other symbols: same conventions as Fig. 1.

periodic orbits are due to the delayed feedback control and we call them control modes. Normally, they have higher frequency and therefore correspond to multiple roundtrips in the delay loop. When the Pyragas mode and the orbits generated in such saddle-node bifurcations intersect a transcritical bifurcation may be caused, where the stability of both states interchange. The information contained in the two-dimensional diagrams are actually data obtained by a projection of higher dimensional manifolds. Thus, not all such intersections correspond to transcritical bifurcations since distinct orbits can be involved.

In what follows we will mainly concentrate on the presentation in the (β, Ω)-projection, like in Fig. 1, panel (a). The respective bifurcations in the (β, R) projection, panel (b), can easily be identified by the their value of β. For a suitable choice of parameters a particular control mode may become stable. In the saddle-node bifurcation at $(\beta, \Omega) \approx (-0.66\pi\,, 0.13)$ [panel (a)] and $(\beta, R) \approx (0.31\,, 0.13)$ [panel (b)] a pair of control modes is born both of which are initially unstable. The lower branch, the node-type control mode, has one positive eigenvalue less than the dimension the upper branch. The latter branch, the saddle-type control mode, stabilises in a Hopf bifurcation at $(\beta, \Omega) \approx (-0.1\pi\,, 0.65)$ as the control phase increases. Furthermore, at $(\beta, \Omega) \approx (0.06\pi\,, 0.78)$ this control mode intersects the Pyragas mode and stability is interchanged in a transcritical bifurcation ($\circ$). Thus, the onset respectively the breakdown of Pyragas control is accompanied by a locking or drift of the frequency of the stable oscillation. As the control phase β is increased further, the amplitude of the control mode decreases until it disappears in a Hopf bifurcation ($\bullet$) of the trivial solution at $(\beta, \Omega) \approx (0.19\pi\,, 0.89)$. The node-type control mode finally intersects the Pyragas mode as well in a second transcritical bifurcation, but none of them gains stability since the latter has already lost its stability in a Hopf bifurcation. Eventually, the node-type control mode stabilises in a Hopf bifurcation at $(\beta, \Omega) \approx (1.5\pi\,, 0.11)$, before disappearing in Hopf bifurcation of the trivial solution at $(\beta, \Omega) \approx (1.6\pi\,, 1.29)$.

Additional control modes with shorter period are born and destroyed in saddle-node bifurcations. In the (β, Ω)-projection they form closed loops, so-called control mode components, with a saddle-node bifurcation at the left and the right turning points. The upper and lower part of the component consists of a saddle-type and a node-type mode, respectively. For the chosen values of the fixed parameters λ and γ these components are unstable.

We supplement the one-parameter bifurcation analysis by data for fixed phase and varying control amplitude. Figure 2 shows the result at $\beta = 2/3\pi$. Again, the Pyragas mode can be identified as the horizontal line at $\Omega \approx 0.79$. Just as in Fig. 1, the Pyragas mode stabilises in a transcritical bifurcation at the intersection with the first control mode, see enlarged view of panel (b). Additional control modes are born in saddle-node bifurcations when the control strength is tuned away from zero and these modes can undergo additional Hopf bifurcations. As can be seen from panel (a), the number of control modes increases when $|K|$ becomes larger, therefor substantially increasing the complexity of the system. Furthermore, it should be noted that typically additional control modes are unstable. Thus, increasing the control strength does not result in increasing stability of the system.

In addition, Fig. 2 shows how the location of the saddle-node bifurcation points (+) change when the control phase β changes. Such a representation corresponds to the projection of a two-parameter bifurcation analysis onto

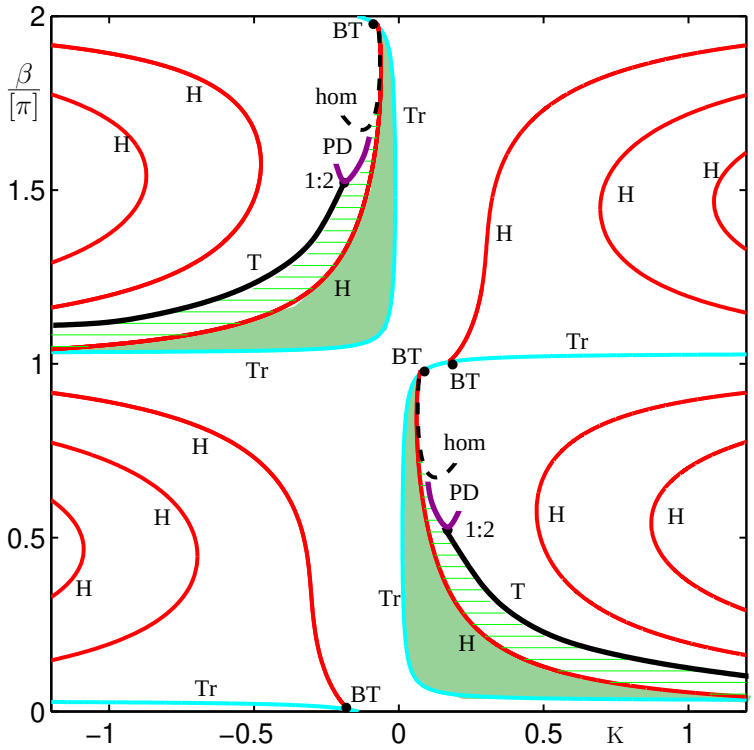

Fig. 3. Two-parameter bifurcation diagram of the Pyragas mode in the (K, β)-projection. Stability region of the Pyragas mode (green/shaded), stability region of the bifurcating periodic orbit (green/hatched). Transcritical bifurcation (Tr), Hopf bifurcation (H), torus bifurcation (T), period-doubling bifurcation (PD), homoclinic bifurcations (hom), 1:2-resonance (1:2), Bogdanov-Takens points (BT).

the (K, Ω)-plane. The light blue curves are the projection of the saddle-node bifurcation manifold along the β-axis onto the (K, Ω)-plane. Similarly, the projection of the Hopf bifurcation manifold of the trivial solution is shown in gray. In particular, the saddle-node bifurcation of the first control mode hits the Hopf bifurcation of the trivial solution at $(K, \Omega) \approx (0.02, 0.99)$. This point can be identified as a degenerate Hopf point which marks the transition from a supercritical to a subcritical bifurcation of the trivial solution.

4 Stability domains

As already indicated in Fig. 2 a two parameter bifurcation analysis is desirable, with respect to the control parameters K and β. Since the first control mode is responsible for the stability changes of the Pyragas mode we will concentrate on these two states. Figure 3 shows the complete two parameter bifurcation diagram of the Pyragas mode and Fig. 4 of the first control mode in the (K, β)-projection. Note the π-translational symmetry involving the parameters β and K, according to Eq. (5). Thus, in what follows we will only discuss the

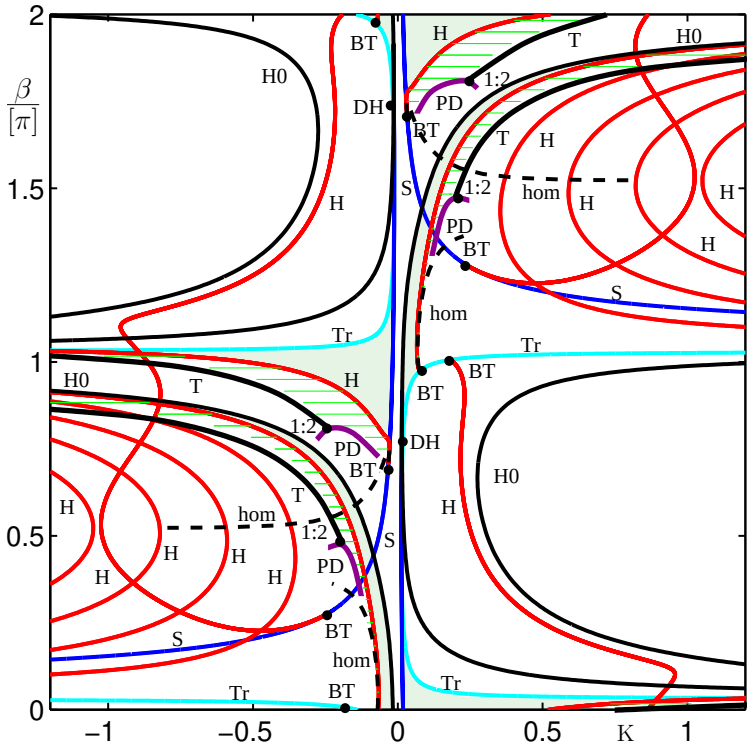

Fig. 4. Two-parameter bifurcation diagram of the first control mode in the (K, β)-projection. Stability region of the control mode (green/shaded), stability region of the bifurcating periodic orbit (green/hatched). Saddle-node bifurcation (S), Hopf bifurcation of the trivial solution (H0), degenerate Hopf point (DH), and the same notation as in Fig. 3 for the other labels.

positive half plane $K \geq 0$ of the bifurcation diagram Fig. 3. Moreover, β can be restricted to the fundamental 2π-interval.

In Fig. 3, the shaded areas indicate the regions for linear stability of the Pyragas mode in the (K, β)-projection. The domain is bounded by a transcritical bifurcation (Tr) at low values of $|K|$. At this boundary the Pyragas mode intersects the first control mode and their stability interchanges. At large values of $|K|$ the stability domain is bounded by a Hopf bifurcation curve (H). The Hopf curve terminates on the transcritical bifurcation curve in a degenerate Bogdanov-Takens point (BT).

Beyond the Hopf boundary the constant amplitude R_P of the Pyragas mode starts to oscillate. In the frame rotating with the Pyragas frequency Ω_P this appears as a periodic orbit. The hatched areas in Fig. 3 indicate the stability regions of the bifurcating periodic orbit. As typical for a Bogdanov-Takens point in its vicinity the period of the bifurcating periodic orbit tends to infinity, indicating a homoclinic bifurcation (hom), which is a global bifurcation. In our case the homoclinic bifurcation is generated by an intersection of the stable and the unstable manifold of the Pyragas mode. This aspect will be

discussed in more detail in Sec. 5. Further away from the Bogdanov-Takens point the periodic orbit destabilises in period-doubling bifurcations (PD) or torus bifurcations (T). The curve of torus bifurcations does not show phase locking because of the S^1-symmetry of the system. But there occurs a 1:2-resonance (1:2) where the torus curve terminates and hits the period doubling curve as the control phase β is increased.

Additional Hopf instabilities of the already unstable Pyragas mode are indicated as well (H). Two of these curves terminate at degenerate Bogdanov-Takens points (BT) at the transcritical bifurcation. Fig. 3 shows that for $\beta = n\pi$ there is no stable Pyragas mode, in accordance with analytical estimates.

At the transcritical bifurcation curve the Pyragas mode exchanges stability with the first control mode. Figure 4 shows the complete two-parameter bifurcation diagram of the first control mode component in the (K, β)-projection. As before, we can just confine the discussion to the region $K \geq 0$.

Modes of the first control mode component are born in pairs in saddle-node bifurcations (S). Comparison with Fig. 2 shows how the frequency Ω of the bifurcating control mode changes along the saddle-node curve (S). Eventually, the modes on this first component disappear in a Hopf bifurcation (H0) of the trivial solution. The latter bifurcation changes from supercritical to subcritical in degenerate Hopf points (DH) where the saddle-node curve ends on (H0). Additional Hopf (H) curves of the already unstable control mode are found as well.

In Fig. 4, the shaded regions indicate the stability of the first control mode and the hatched region stability of the bifurcating periodic solution. There are two stability regions of the first control mode. For large values of the control phase β a stable control mode bifurcates from a Hopf bifurcation (H0) of the trivial solution. As the control strength K is increased this mode destabilises in a Hopf bifurcation (H). For smaller values of the control phase a pair of control modes appears in a saddle-node bifurcation (S) and one of them is stable. Depending on the value of the control phase β the stable control mode changes stability in a transcritical bifurcation (Tr) at the intersection with the Pyragas mode or it destabilises in a Hopf bifurcation (H). Similar to the bifurcation scenario of the Pyragas mode, as the control strength increases, the bifurcating periodic solution destabilises in torus (T) or period-doubling (PD) bifurcations, depending on the value of the control phase. Again the torus curve ends in a 1:2-resonance (1:2) when hitting the period-doubling curve. Close to the Bogdanov-Takens point the period of the bifurcating periodic orbit tends to infinity, indicating a homoclinic orbit.

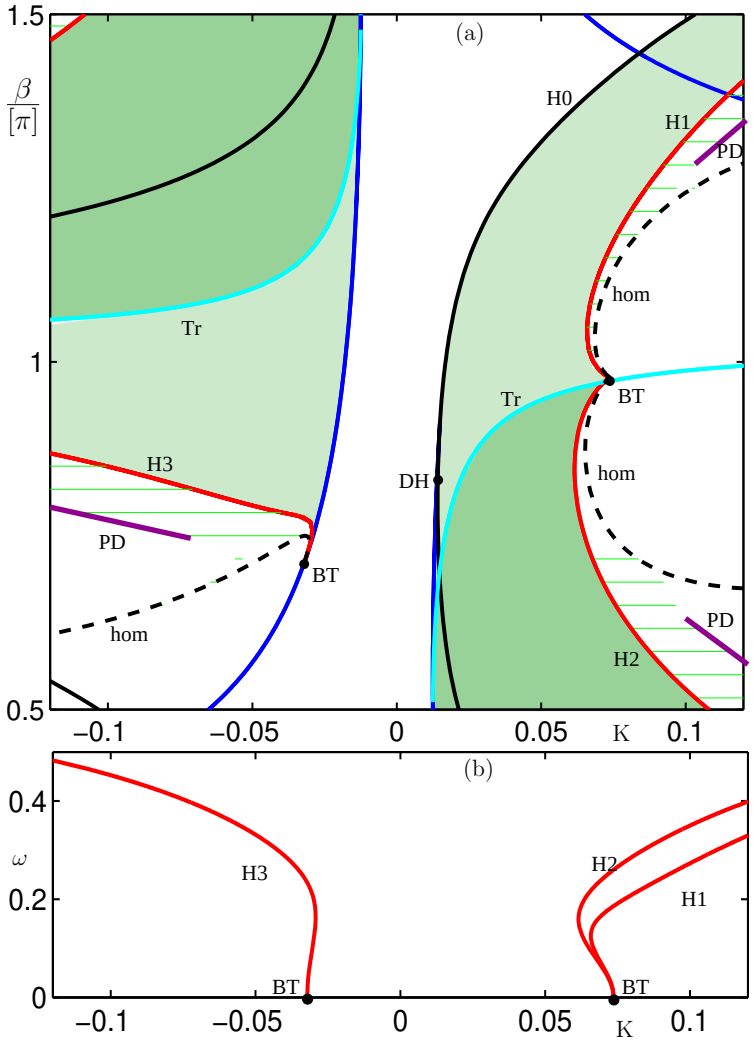

Fig. 5. (a): Enlarged view of the two-parameter bifurcation diagram around the Bogdanov-Takens points in the (K, β)-projection, including bifurcations of the Pyragas mode and the first control mode. Stability region of the Pyragas mode in dark green shading; stability region of the control mode in light green shading. Homoclinic bifurcations (hom) black dashed curve, and the same notation as in Fig. 3 for the other labels. (b): Dependence of the imaginary part of the eigenvalue along the different Hopf bifurcation curves (H1), (H2), and (H3) (cf. panel (a)) on the control amplitude K.

5 Dynamics close to the Bogdanov-Takens points

We now focus on the dynamics emerging from the Bogdanov-Takens points. Figure 5(a) shows an enlarged view of the two-parameter bifurcation diagram in the (K, β)-projection in a neighbourhood of the two Bogdanov-Takens points (BT). This diagram now includes both, the bifurcations of the Pyragas mode and of the first control mode (cf. Figs. 3 and 4).

First, we concentrate on the Bogdanov-Takens point caused by a collision of a Hopf bifurcation and a saddle-node bifurcation at $(K, \beta) \approx (-0.032\,, 0.71\pi)$. As required by bifurcation theory (see for example Ref. [14]) there emerges a Hopf bifurcation (H3) from such a generic Bogdanov-Takens point. Figure 5(b) shows the imaginary part ω of the associated eigenvalue along this Hopf curve. As the Hopf bifurcation approaches the Bogdanov-Takens point, ω goes to zero. Since ω determines the period $T = 2\pi/\omega$ of the bifurcating periodic orbit, such a period tends to infinity when approaching the Bogdanov-Takens point. Thus, we find a homoclinic bifurcation (hom) emerging from BT, which relates to orbits with an infinite period.

We have detected a second Bogdanov-Takens point at $(K, \beta) \approx (0.073\,, 0.97\pi)$. In this non generic case the Bogdanov-Takens point lies on the transcritical bifurcation curve (Tr). The transcritical bifurcation is a consequence of the Pyragas condition Eq. (4). When this condition is relaxed the transcritical bifurcation may unfold to two saddle-node bifurcations, see for example Ref. [21]. As can be seen from Fig. 5(a) there are two Hopf curves and two homoclinic curves emerging from this degenerated Bogdanov-Takens point. Again Fig. 5(b) shows the imaginary part ω of the associated eigenvalue along these Hopf curves (H1) and (H2). Both frequencies tend to zero when the Bogdanov-Takens point is approached.

Both Bogdanov-Takens points are as well located on the boundary of the stability domains of the Pyragas and the control mode, respectively. In particular, the degenerated Bogdanov-Takens point links to both, the stability domains of the Pyragas and the control mode, as well as to the stability domain of the quasiperiodic state. Thus, these higher codimension bifurcation points may be considered as the organising centre for time-delayed feedback control in the present setup. The stability domain of the quasiperiodic state is bounded by a homoclinic bifurcation close to the Bogdanov-Takens point. At larger distances we find a change in the nature of such a boundary since now periodic orbits bifurcate in period-doubling bifurcations (PD). The detailed bifurcation structure around the transition region between the period-doubling and the homoclinic bifurcations would include other bifurcations of mainly unstable periodic orbits, such as torus bifurcations and saddle-node bifurcations of limit cycles. The detailed investigation of such features is beyond the scope of the present study. To uncover the details a careful unfolding of the underlying higher codimension bifurcation would be fruitful.

Here, instead, we show an example for a periodic orbit close to a homoclinic bifurcation for $(K, \beta) = (0.15\,, 0.68\pi)$ (cf. Fig. 6). A homoclinic bifurcation, also known as a homoclinic connection, is a global bifurcation where the unstable and stable manifold of a phase-space object, such as a fixed point or a periodic solution, connect [14]. In our example the unstable and stable manifold of the Pyragas mode connect in a homoclinic bifurcation. Panel (a) shows the time

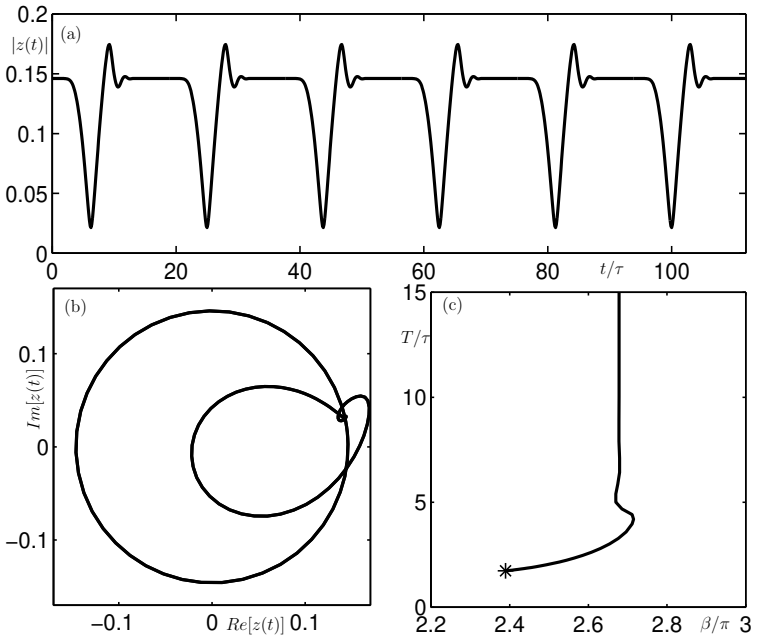

Fig. 6. A periodic orbit close to a homoclinic bifurcation at $(K, \beta) = (0.15\,, 0.68\pi)$: time series in panel (a) and phase portrait in panel (b). (c): One-parameter bifurcation diagram of the periodic solution for $K = 0.15$, approaching a homoclinic bifurcation at $\beta \approx 0.68\pi$.

series of the amplitude $|z(t)|$, where time t is given in units of the delay time τ. Panel (b) shows the corresponding trajectory in the $(\mathrm{Re}[z(t)], \mathrm{Im}[z(t)])$-plane, i.e. a projection of the infinite-dimensional phase space. The trajectory can be separated into two parts. In the first part $|z(t)|$ is almost constant and close to the weakly unstable Pyragas mode. Eventually, the trajectory leaves the vicinity of the Pyragas mode by initially following the associated unstable manifold. The trajectory approaches the Pyragas mode again via its stable manifold. This large phase space excursion can be seen as an oscillation in the time series in panel (a). As the periodic orbit gets even closer to the homoclinic connection, the time which the trajectory spends near the Pyragas mode increases, thus increasing its period. Panel (c) shows a one-parameter bifurcation diagram of the periodic orbit approaching the homoclinic bifurcation, where we plot the period T as a function of the bifurcation parameter β. The periodic orbit is born in a Hopf bifurcation ($*$) and as β changes, indeed, the period grows swiftly.

6 Conclusions

We have presented a comprehensive bifurcation analysis of a generic nonlinear oscillator model subjected to time-delayed feedback control. In particular, we have demonstrated how the increasing complexity of the solution structure

is organised by saddle-node bifurcations, giving rise to an increasing number of coexisting control modes. Regions of bistability between the trivial fixed point $z = 0$ and the Pyragas mode, which have been reported recently [11] have been confirmed as well. While such a bifurcation analysis is not able to capture, a priori, global stability properties like basins of attraction, we have obtained a global overview of the local linear stability properties of all the states involved in time-delayed feedback control. With regards to the stability of the Pyragas mode, we have shown that for finite values of the phase β a finite control domain appears. The domain is bounded by a transcritical bifurcation and a Hopf bifurcation for small and large control amplitudes, respectively. At the transcritical boundary a stable control mode is generated which is reflected by a continuous shift in the period of the signal. The stability domain of this control mode includes the case of vanishing phase, $\beta = 0$, and the whole domain is connected to the control domain of the Pyragas mode. Thus, an appropriate adiabatic shift of control parameters yields successful control of the desired target state whenever a periodic output signal has been generated. At the upper boundary of the control domain a stable quasiperiodic torus solution is generated. On further increase of the control amplitude such a state is destabilised in a torus- or a period doubling bifurcation, depending on the control phase. No phase locking occurs in this model due to the rotational symmetry. For large values of the control amplitude no stability region is found, neither for periodic nor for quasiperiodic solutions. The sequence of Hopf bifurcations for the Pyragas mode and the first control mode indicate a higher dimensional unstable manifold and complex dynamical behaviour is expected to occur.

From the plain theoretical point of view the model shows quite interesting bifurcations of higher codimension, subjected to a symmetry which forces the genericity of the transcritical bifurcation. We identified several codimension-two points, such as degenerate Hopf points and Bogdanov-Takens points in the parameter plane of control phase and control strength. Specifically, the Bogdanov-Takens points give rise to homoclinic bifurcations and the points serve as organising centres for the whole bifurcation diagram. Applying the same type of analysis to other models of time-delayed feedback control can uncover yet unknown global properties of the control scheme. But we expect that our bifurcation diagrams exhibit a substantial degree of structural stability. In particular, the identification of large stability regions with regards to control parameters which are directly accessible in applications, and the transitions involved at the stability boundary and their physical manifestation can significantly facilitate experimental confirmations.

Acknowledgements

The authors acknowledge financial support through the European Commissions NEST programme by the project MANMADE (Contract No 043363)

References

[1] *Handbook of Chaos Control (2nd edition)*, edited by E. Schöll and H. G. Schuster (Wiley-VCH, Weinheim, 2007).

[2] K. Pyragas, *Continuous control of chaos by self–controlling feedback*, Phys. Lett. A **170**, 421 (1992).

[3] M. C. Mackey and L. Glass, *Oscillation and chaos in physiological control system*, Science **197**, 287 (1977).

[4] M. Dhamala, V. K. Jirsa, and M. Ding, *Enhancement of neural synchrony by time delay*, Phys. Rev. Lett. **92**, 074104 (2004).

[5] D. V. R. Reddy, A. Sen, and G. L. Johnston, *Experimental evidence of time-delay-induced death in coupled limit-cycle oscillator*, Phys. Rev. Lett. **85**, 3381 (2000).

[6] A. P. A. Fischer, M. Yousefi, D. Lenstra, M. W. Carter, and G. Vemuri *Filtered optical feedback induced frequency dynamics in semiconductor lasers*, Phys. Rev. Lett. **92**, 023901 (2004).

[7] S. Schikora, P. Hövel, H.-J. Wünsche, E. Schöll, and F. Henneberger, *All-optical noninvasive control of unstable steady states in a semiconductor laser*, Phys. Rev. Lett. **97**, 213902 (2006).

[8] M. E. Bleich and J. E. S. Socolar, *Stability of periodic orbits controlled by time–delayed feedback*, Phys. Lett. A **210**, 87 (1996).

[9] W. Just, T. Bernard, M. Ostheimer, E. Reibold, and H. Benner, *Mechanism of time-delayed feedback control*, Phys. Rev. Lett. **78**, 203 (1997).

[10] H. Nakajima, *On analytical properties of delayed feedback control of chaos*, Phys. Lett. A **232**, 207 (1997).

[11] B. Fiedler, V. Flunkert, M. Georgi, P. Hövel, and E. Schöll, *Refuting the odd number limitation of time-delayed feedback control*, Phys. Rev. Lett. **98**, 114101 (2007).

[12] W. Just, B. Fiedler, M. Georgi, V. Flunkert, P. Hövel, and E. Schöll, *Beyond the odd number limitation: a bifurcation analysis of time-delayed feedback control*, Phys. Rev. E **76**, 026210 (2007).

[13] C. v. Loewenich, H. Benner, and W. Just, *Experimental relevance of global properties of time-delayed feedback control*, Phys. Rev. Lett. **93**, 174101 (2004).

[14] *Nonlinear Oscillations, Dynamical Systems, and Bifurcations of Vector Fields*, J. Guckenheimer and Holms (Springer-Verlag, New York, 1986).

[15] M. Rosenblum and A. Pikovsky *Delayed feedback control of collective synchrony: An approach to suppression of pathological brain rhythms* Phys. Rev. E **70**, 041904 (2000).

[16] T. Heil, I. Fischer, W. Elsäßer, B. Krauskopf, K. Green, and A. Gavrieldies, *Delay dynamics of semiconductor lasers with short external cavities: bifurcation scenarios and mechanisms*, Phys. Rev. E **67**, 066214 (2003).

[17] H. Erzgräber, D. Lenstra, B. Krauskopf, A. P. Fischer, and G. Vemuri *Feedback phase sensitivity of a semiconductor laser subject to filtered optical feedback: Experiment and theory* Phys. Rev. E **76**, 026212 (2007).

[18] K. Engelborghs, T. Luzyanina, and G. Samaey, *DDE-BIFTOOL v. 2.00: a Matlab package for bifurcation analysis of delay differential equations*, Department of Computer Science, K. U. Leuven, Belgium (available from http://www.cs.kuleuven.ac.be/publicaties/rapporten/tw/TW330.abs.html), 2006.

[19] H. Erzgräber, B. Krauskopf, and D. Lenstra, *Bifurcation analysis of a semiconductor laser with filtered optical feedback*, SIAM J. Appl. Dyn. Sys. **6**, 1 (2007).

[20] A. G. Balanov, N. B. Janson, and E. Schöll, *Delayed feedback control of chaos: Bifurcation analysis*, Phys. Rev. E **71**, 016222 (2005).

[21] *Elements of Applied Bifurcation Theory*, Yu. A. Kuznetsov (Springer-Verlag, New York, 1995).